

Improving Semantic Uncertainty Quantification in LVLMs with Semantic Gaussian Processes

Joseph Hoche¹Andrei Bursuc²David Brellmann³Gilles Louppe⁴Pavel Izmailov⁵Angela Yao⁶Gianni Franchi^{1,7}

¹AMIAD, Pôle Recherche, Palaiseau ²valeo.ai ³Safran Tech ⁴University of Liège
⁵New York University ⁶National University of Singapore ⁷ENSTA Paris

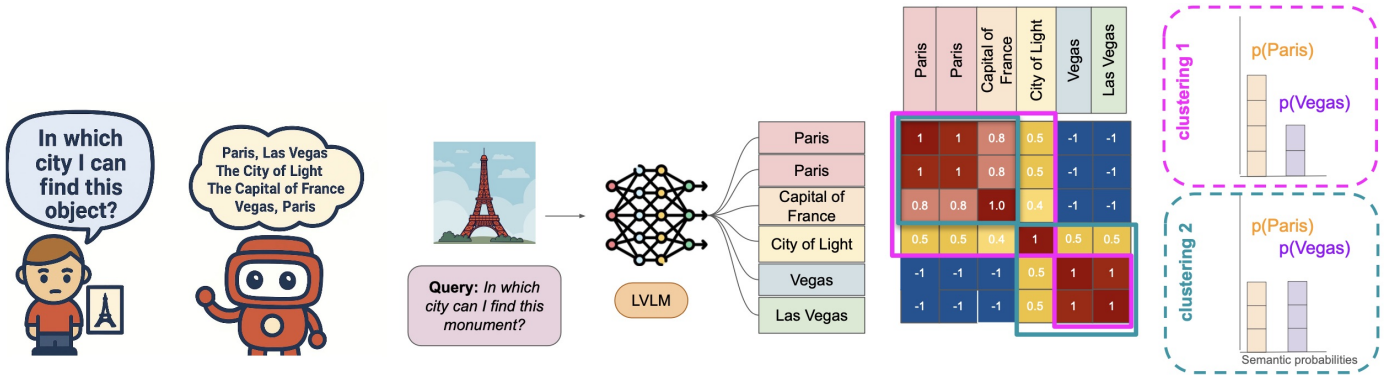


Figure 1. **Illustration of semantic uncertainty quantification in LVLMs using clustering strategies.** Instead of generating a single response, multiple responses are sampled to assess semantic uncertainty. Two possible clusterings are shown in pink and green: in the pink example, the model appears more confident because the Paris cluster dominates, whereas in the green partition both clusters are of similar size, indicating higher uncertainty. The uncertainty scores vary depending on how these outputs are semantically grouped.

Abstract

Large Vision-Language Models (LVLMs) often produce plausible but unreliable outputs, making robust uncertainty estimation essential. Recent work on semantic uncertainty estimates relies on external models to cluster multiple sampled responses and measure their semantic consistency. However, these clustering methods are often fragile, highly sensitive to minor phrasing variations, and can incorrectly group or separate semantically similar answers, leading to unreliable uncertainty estimates. We propose **Semantic Gaussian Process Uncertainty (SGPU)**, a Bayesian framework that quantifies semantic uncertainty by analyzing the geometric structure of answer embeddings, avoiding brittle clustering. SGPU maps generated answers into a dense semantic space, computes the Gram matrix of their embeddings, and summarizes their semantic configuration via the eigenspectrum. This spectral representation is then fed into a Gaussian Process Classifier that learns to map patterns of semantic consistency to predictive uncertainty, and that

can be applied in both black-box and white-box settings. Across six LLMs and LVLMs on eight datasets spanning VQA, image classification, and textual QA, SGPU consistently achieves state-of-the-art calibration (ECE) and discriminative (AUROC, AUROC) performance. We further show that SGPU transfers across models and modalities, indicating that its spectral representation captures general patterns of semantic uncertainty.

1. Introduction

Large Vision-Language Models (LVLMs) extend Large Language Models (LLMs) to multimodal inputs and are now used for tasks requiring both visual comprehension and language understanding [25, 68, 79, 81, 82]. Despite their success, LVLMs are prone to hallucinations, generating content that appears plausible but factually incorrect or unfaithful to the input [31, 33, 56]. This raises the need for reliable uncertainty quantification (UQ) to detect when

generated content should not be trusted [2, 21, 29, 42]. Existing UQ methods for LVLMs and LLMs mostly fall into two families: token-based measures, which operate directly on autoregressive token probabilities (e.g., log-perplexity or predictive entropy) [3, 60], and *semantic uncertainty* measures, which attempt to quantify variability in the meaning of multiple sampled responses, typically by grouping outputs in a semantic space using external semantic models and clustering techniques [1, 12, 18, 35, 48, 67].

Figure 1 illustrates the limitations of these approaches on a visual question answering example. Given the question “*In which city can I find this monument?*”, an LVLM may generate several answers that all refer to Paris (e.g., “*The figure shows the Eiffel Tower in Paris.*” and “*The Eiffel Tower is depicted in this image.*”). Token-based scores may assign different uncertainties to these phrases due to lexical and syntactic differences, even though they are semantically equivalent [3]. Semantic uncertainty methods aim to address this by comparing multiple sampled responses in a semantic space, using external models such as Natural Language Inference (NLI) systems, instruction-tuned LLMs, or sentence encoders, and by grouping responses into semantic clusters to estimate how often the model “changes its mind” about the answer [18, 41]. When the model instead produces conflicting answers (e.g., Paris, Las Vegas, Tokyo), semantic uncertainty should be high. However, in practice, the semantic comparison and clustering steps are fragile: small changes in phrasing, additional correct details, or uninformative tokens can perturb similarity scores, splitting truly equivalent answers or merging semantically distinct ones [23, 48, 66]. As a consequence, the estimated semantic uncertainty can be inconsistent and sensitive to the choice of external model, similarity metric, and comparison heuristic.

An alternative to explicit clustering is to analyze the geometric structure of generated responses within a dense semantic space rather than on discrete tokens [11, 32, 38, 43, 78]. This line of works measure semantic consistency by computing properties of the answer embeddings, such as the eigenvalues of their covariance matrix or Gram matrix [11, 43, 78]. Such approaches capture the volume or spread of the answers in the embedding space as a proxy for uncertainty. This semantic space can be derived from the hidden activations of the model (a white-box approach) [4, 38, 48, 69] or from an external sentence encoder (a black-box approach) [43], offering greater flexibility. By analyzing the overall structure of the answer space rather than partitioning it, these methods avoid the brittleness of explicit clustering. However, most approaches typically rely on heuristic scores or discriminative probes learned on top of the representations, without a principled probabilistic treatment of semantic uncertainty.

In this work, we introduce *Semantic Gaussian Process*

Uncertainty (SGPU), a Bayesian framework for semantic UQ in LVLMs that operates directly on the geometry of answer embeddings. Given an input (image and/or text), we sample multiple answers from an LVLM and embed each answer in a dense semantic space using a sentence encoder. We then construct a Gram matrix over these embeddings and summarize the semantic configuration of the answers by its eigenspectrum. This eigenspectrum serves as a compact descriptor of the semantic consistency. Intuitively, a spectrum dominated by a few large eigenvalues corresponds to a low-dimensional, concentrated semantic manifold (high semantic consistency), whereas a flatter spectrum indicates dispersed, semantically diverse answers (high semantic uncertainty). SGPU feeds this spectral representation into a *Gaussian Process Classifier* (GPC), which learns to map patterns of semantic consistency to predictive confidence. As the encoder is external, SGPU can be applied both to white-box and fully black-box LVLMs, and the GPC provides a principled Bayesian model that yields calibrated uncertainty estimates from simple, low-dimensional features.

Our contributions are threefold. (1) We introduce Semantic Gaussian Process Uncertainty (SGPU), a novel Bayesian framework for semantic uncertainty quantification in LVLMs that avoids explicit clustering and operates on the eigenspectrum of answer embeddings. (2) We demonstrate through extensive benchmarks (involving six LLMs and LVLMs across eight datasets) that SGPU consistently achieves state-of-the-art performance in both uncertainty calibration and discrimination. (3) We show that SGPU exhibits strong transfer across models, datasets, and modalities, indicating that the learned spectral representation captures general semantic uncertainty patterns that can be reused beyond the training setting. Furthermore, we observe that SGPU provides a direct characterization of the uncertainty of its prediction, which enables to detect cases where SGPU is uncertain.

2. Related Works

Bayesian Uncertainty Estimation. Uncertainty quantification has long been a central topic in Bayesian machine learning [63], originating with probabilistic models such as Gaussian Processes (GPs) [85] that provide elegant, analytically tractable posterior inference. These early Bayesian methods inspired the development of Bayesian Neural Networks (BNNs) [57, 58, 65], which extend the Bayesian framework to deep architectures by placing priors over neural network weights.

Recent research has revisited BNNs in the context of modern deep learning, proposing scalable approximations that make Bayesian inference feasible for large models and datasets [9, 21, 47]. Despite impressive progress, these methods remain computationally demanding and often struggle to scale to high-dimensional vision tasks. This

limitation has motivated specialized Bayesian formulations for computer vision, leveraging architectural adaptations and more efficient posterior approximations [19, 59].

An alternative family of approaches sidesteps explicit posterior computation through model ensembling [20, 42, 46, 84], which empirically captures epistemic uncertainty without relying on explicit priors. Another influential line of work leverages the Laplace approximation [15, 74], which provides a second-order, tractable estimate of the posterior around a mode of the loss landscape. This family of methods has recently gained renewed interest for their ability to yield calibrated uncertainty estimates even in large-scale vision models [7]. However, despite these advances, most Bayesian and approximate Bayesian approaches have been developed for non-generative architectures. Their direct application to LVLMs and LLMs remains challenging due to the models’ size, multimodal nature, and complex latent representations. This motivates our work.

Uncertainty Quantification in LLM and LVLM. Several recent methods have been proposed to enhance reliability by estimating uncertainty in the predictions of LLMs and LVLMs. These include approaches that ask the LVLM itself for its confidence [13, 14, 37, 53, 61]; methods that estimate uncertainty based on internal representations and token-level confidence from single generations [4, 8, 17, 50, 60, 64, 69, 73]; techniques that assess uncertainty through response changes under perturbations [22, 52, 87]; and methods that estimate uncertainty by measuring their consistency across multiple generated responses via their semantics using external models, internal representations and confidence scores [1, 18, 23, 35, 41, 43, 48, 54, 60, 67, 70]. Our method belongs to the last category by quantifying semantic uncertainty by measuring consistency between responses with an external sentence embedding model and leveraging GPC.

3. Preliminaries

Given an input x which may contain images and/or text, an LVLM parameterized by θ autoregressively generates an output response sequence of tokens $\mathbf{y} = \{\mathbf{y}_t\}_{t=1}^T$, where \mathbf{y}_t denotes the t^{th} output token and T is the length of the output sequence. The probability of the generated sequence \mathbf{y} is the joint probability of tokens, defined as the product of conditional token probabilities:

$$p(\mathbf{y} | \mathbf{x}, \theta) = \prod_{t=1}^T p(\mathbf{y}_t | \mathbf{x}, \mathbf{y}_{<t}, \theta), \quad (1)$$

where $\mathbf{y}_{<t} = \{\mathbf{y}_1, \dots, \mathbf{y}_{t-1}\}$.

3.1. Uncertainty Estimation

Log-Perplexity. A straightforward uncertainty measure is the average negative log-likelihood of generated tokens or

the log-perplexity [60, 64]. Log-perplexity is defined as the arithmetic mean of the log-probabilities of the generated tokens:

$$\begin{aligned} \log \text{PPL}(\mathbf{y} | \mathbf{x}, \theta) &= -\frac{1}{T} \sum_{t=1}^T \log p(\mathbf{y}_t | \mathbf{x}, \mathbf{y}_{<t}, \theta) \\ &= -\frac{1}{T} \log p(\mathbf{y} | \mathbf{x}, \theta). \end{aligned} \quad (2)$$

Predictive Entropy. Another common baseline inspired from classification tasks [2] is the predictive entropy [18, 37, 54]. Given an input x , the predictive entropy is defined as the mean log-perplexity computed over a set of N generated candidate sequences $\mathcal{Y} := \{\mathbf{y}^{(1)}, \dots, \mathbf{y}^{(N)}\}$:

$$H(\mathcal{Y} | \mathbf{x}, \theta) = \frac{1}{N} \sum_{i=1}^N \log \text{PPL}(\mathbf{y}^{(i)} | \mathbf{x}, \theta). \quad (3)$$

$H(\mathcal{Y} | \mathbf{x}, \theta)$ provides a Monte-Carlo approximation of the Shannon entropy $\mathbb{E}_{\mathbf{y}}[-\log p(\mathbf{y} | \mathbf{x}, \theta)]$ over outputs generated by the LVLM. The log-perplexity and the predictive entropy reach their highest values when the output is uncertain within the token space.

Semantic Entropy. Given an input x , the semantic entropy is defined over a set of generated sequences $\mathcal{Y} := \{\mathbf{y}^{(1)}, \dots, \mathbf{y}^{(N)}\}$ that are partitioned into semantically consistent clusters $\mathcal{C} := \{\mathcal{C}_k\}_{k=1}^K$, such that sequences within each cluster share the same meaning. In practice, clustering is performed either by using bidirectional entailment predictions from NLI models [18, 41, 67] and instruction-tuned LLMs [18, 34, 67] or by using embeddings derived from hidden states of the LVLM [48] and external models [1]. The probability mass $p(\mathcal{C}_k | \mathbf{x}, \theta)$ assigned to each cluster \mathcal{C}_k is defined as the sum of normalized sequence probabilities of all outputs assigned to that cluster as:

$$p(\mathcal{C}_k | \mathbf{x}, \theta) = \sum_{\mathbf{y} \in \mathcal{C}_k} \tilde{p}(\mathbf{y} | \mathbf{x}, \theta), \quad (4)$$

where $\tilde{p}(\mathbf{y} | \mathbf{x}, \theta) = \frac{p(\mathbf{y} | \mathbf{x}, \theta)}{\sum_{i=1}^N p(\mathbf{y}^{(i)} | \mathbf{x}, \theta)}$ for $\mathbf{y} \in \mathcal{Y}$. Using the Rao-Blackwellized Monte Carlo estimator, the semantic entropy [18, 41] is approximated as:

$$H_{\text{SE}}(\mathcal{Y} | \mathbf{x}, \theta) = -\sum_{k=1}^K p(\mathcal{C}_k | \mathbf{x}, \theta) \log p(\mathcal{C}_k | \mathbf{x}, \theta) \quad (5)$$

and measures the dispersion of probability mass across distinct meanings. A low H_{SE} value indicates that the model responses are tightly clustered around a single meaning, whereas a high H_{SE} value reflects greater semantic diversity in the outputs.

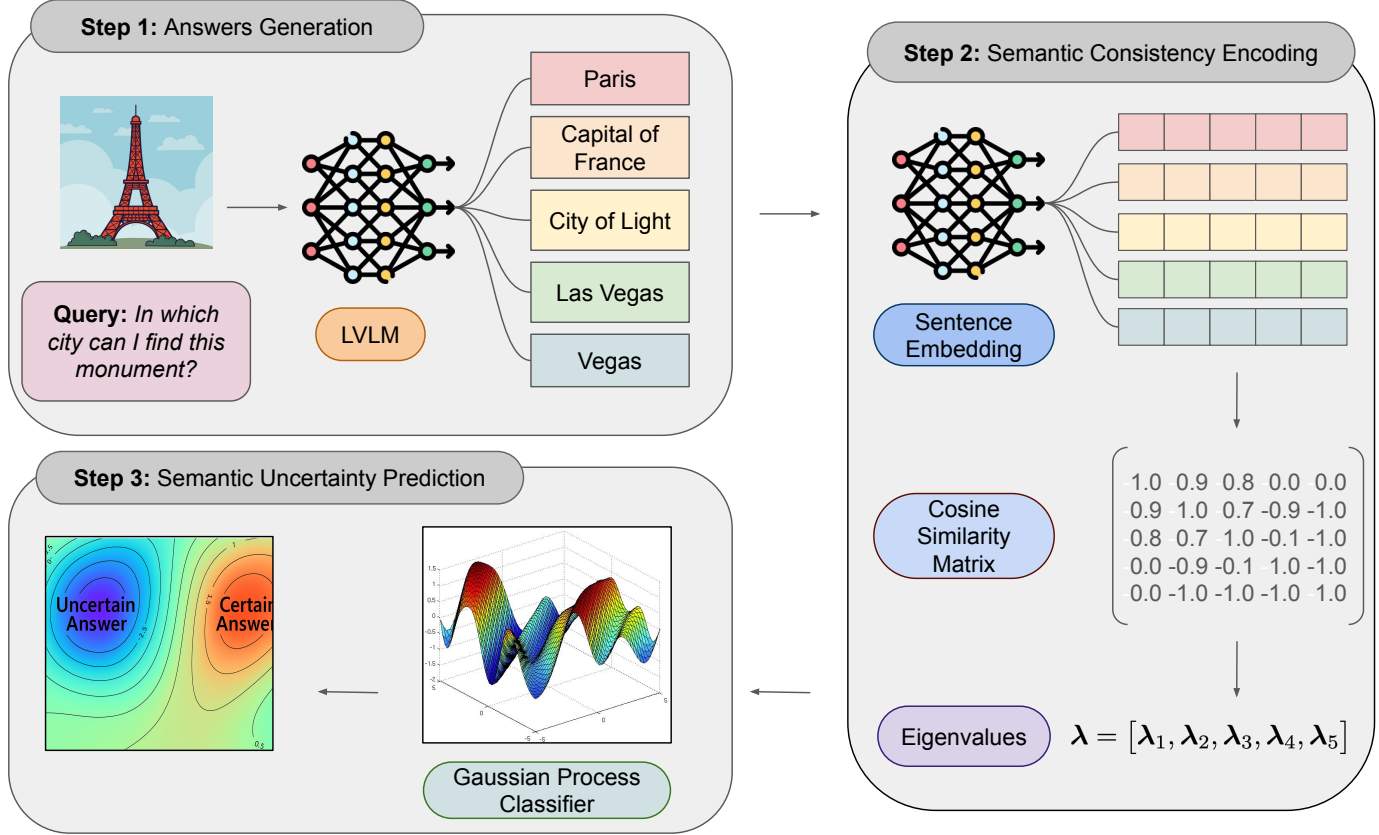


Figure 2. **Illustration of the SGPU pipeline.** SGPU operates in three steps: (1) generating multiple candidate sequences for a given context (query + image), (2) encoding their semantic consistency into a single vector representation λ , and (3) using this vector representation as input for a Gaussian Process classifier to estimate the predictive semantic uncertainty / truthfulness of the generated samples.

Discrete Semantic Entropy. Discrete semantic entropy [18, 41] is another extension of semantic entropy for black-box LVLMs. It approximates the probability mass $p(\mathcal{C}_k \mid \mathbf{x}, \theta)$ assigned to each cluster \mathcal{C}_k with the empirical cluster probability $|\mathcal{C}_k|/n$, yielding:

$$H_{\text{DSE}}(\mathcal{Y} \mid \mathbf{x}, \theta) = - \sum_{k=1}^K \frac{|\mathcal{C}_k|}{n} \log \frac{|\mathcal{C}_k|}{n}. \quad (6)$$

3.2. Latent Uncertainty Estimation

Instead of assessing uncertainty using token likelihoods, alternative approaches leverage dense semantic information retained within the internal states of LVLMs to measure semantic divergence.

Semantic Volume. Given a context \mathbf{x} and a set of generated candidate sequences $\mathcal{Y} := \{\mathbf{y}^{(1)}, \dots, \mathbf{y}^{(N)}\}$, the semantic volume is defined over the embedding matrix $\Phi = [\phi_1, \phi_2, \dots, \phi_N] \in \mathbb{R}^{d \times N}$, where each $\phi_i \in \mathbb{R}^d$ depicts

the sentence embedding of the generated answer $\mathbf{y}^{(i)}$ within the d -dimensional semantic space of the LVLM. Note that the sentence embedding can be derived either by averaging the token embedding or by taking the last token embedding from a chosen layer or attention head [4, 11, 17, 32, 69]. Let $\Sigma = \Phi^T \left[\mathbf{I}_d - \frac{\mathbf{1}_d \mathbf{1}_d^T}{d} \right] \Phi$ denote the empirical covariance matrix of Φ . The semantic volume¹ is then defined as [11, 76, 88, 89]:

$$V(\mathcal{Y} \mid \mathbf{x}, \theta) = \log \det(\Sigma + \alpha \mathbf{I}_N) = \sum_{i=1}^N \log(\lambda_i), \quad (7)$$

where $\det(\mathbf{X})$ represents the determinant of matrix \mathbf{X} , $\alpha > 0$ is a small regularization term to make Σ full rank, and $\lambda = [\lambda_1, \dots, \lambda_N]$ denotes eigenvalues of the matrix $\Sigma + \alpha \mathbf{I}_N$. Variants instead define Σ using the cosine similarity matrix [43, 52] or the Gram matrix [78] and com-

¹The term ‘‘volume’’ arises from the geometric interpretation that $\det(\Phi^T \Phi)$ is the volume of the parallelepiped spanned by $\{\phi_i\}_{i=1}^n$.

bine Σ with probability responses [43]. The semantic volume can be interpreted as the differential entropy within the sentence-level LVM embedding space [11].

4. Semantic Gaussian Process Uncertainty

In this section, we present the details of our proposed Semantic Gaussian Process Uncertainty (SGPU) framework, which is designed to quantify semantic uncertainty in both black-box and white-box LVMs. The complete pipeline is depicted in Figure 2. We start by generating multiple candidate sequences $\mathcal{Y} := \{\mathbf{y}^{(1)}, \dots, \mathbf{y}^{(N)}\}$ for a given context \mathbf{x} (Step 1). Then, using an external sentence embedding model, we embed each answer in a dense semantic space and encode their semantic consistency into single vector representation (Step 2). Finally, this aggregated representation is passed to a Gaussian Process classifier (GPC), which learns to map patterns of semantic consistency to a binary score indicating confidence in the truthfulness of the generated samples (Step 3). Details of how the semantic consistency of generated answers are encoded are provided in Section 4.1 and the Gaussian Process Classifier is described in Section 4.2.

4.1. Semantic Consistency Encoding

Encoders are specifically trained to derive semantically meaningful sentence [72] and are used in applications such as retrieval [49], classification [72] or clustering [1]. To capture semantic consistency of the generated answers $\mathcal{Y} := \{\mathbf{y}^{(1)}, \dots, \mathbf{y}^{(N)}\}$, we embed thus each generated answer $\mathbf{y}^{(i)}$ in \mathcal{Y} in a dense semantic space using a sentence encoder $E(\cdot)$. For each generated answer $\mathbf{y}^{(i)}$ in \mathcal{Y} , we denote by $\phi_i \in \mathbb{R}^d$ its d -dimensional normalized embedding vector with $\|\phi_i\| = 1$. Sentence embedding can be obtained either by averaging the token embeddings, by using the embedding of the last token, or by taking the embedding of a designated special token. Let $\Phi = [\phi_1, \dots, \phi_N] \in \mathbb{R}^{d \times N}$ depict the embedding matrix of generated answers \mathcal{Y} . To capture how semantically close the different model outputs are in the embedding space, we compute the eigenvalues of the Gram matrix:

$$\Sigma = \Phi^T \Phi \in \mathbb{R}^{N \times N}. \quad (8)$$

Each eigenvalue of Σ represents the variance of generated answers \mathcal{Y} along a particular principal direction [75]. We denote the (nonnegative) eigenvalues of Σ by:

$$\boldsymbol{\lambda} = [\lambda_1, \dots, \lambda_N]^T, \quad \lambda_1 \geq \dots \geq \lambda_N \geq 0 \quad (9)$$

Intuitively, the vector $\boldsymbol{\lambda}$ characterizes the semantic consistency of the generated answers \mathcal{Y} as the eigenvalues of Σ (or equivalently the singular values of Φ) capture the degree of divergence and correlation among their embeddings Φ [11, 77, 78]. A spectrum $\boldsymbol{\lambda}$ dominated by a few

large eigenvalues corresponds to a low-dimensional, concentrated semantic manifold and indicates a high semantic consistency across the generated answers. In contrast, a flatter spectrum $\boldsymbol{\lambda}$ implies that the sentence embedding matrix Φ is spread out across many principal semantic directions and suggests semantically diverse answers with high semantic uncertainty. Thus, $\boldsymbol{\lambda}$ serves as a compact yet rich descriptor of the semantic consistency among the generated answers.

4.2. Semantic Uncertainty Prediction

Following prior works [6, 18, 32, 41, 61], we frame semantic uncertainty evaluation as a binary classification task that predicts whether to rely on model generations for a given context. In particular, our approach leans on the common assumption in semantic uncertainty methods that high semantic consistency among generated responses indicates correctness, whereas significant variation indicates potential hallucinations.

Binary Classification Problem. We assume we have a training dataset $\mathcal{D} := \{\mathbf{x}^{(i)}, \mathcal{Y}^{(i)}\}_{i=1}^M$, where $\mathcal{Y}^{(i)} := \{\mathbf{y}_i^{(1)}, \dots, \mathbf{y}_i^{(N)}\}$ depicts a set of N candidate responses generated by the LVM for the given context $\mathbf{x}^{(i)}$. To frame the problem into a binary classification task, we transform the dataset \mathcal{D} into $\tilde{\mathcal{D}} := \{\boldsymbol{\lambda}^{(i)}, l^{(i)}\}_{i=1}^M$, where $\boldsymbol{\lambda}^{(i)} \in \mathbb{R}^N$ denotes the semantic consistency vector of the generated responses $\mathcal{Y}^{(i)}$ for the given context $\mathbf{x}^{(i)}$ (equation 9) and $l^{(i)}$ is the binary label indicating the correctness of generated answers $\mathcal{Y}^{(i)}$. Correctness of predicted answers is commonly used as a proxy for semantic uncertainty [6, 18, 32, 41, 61] since uncertain generations are less likely to be correct. Following recommendations in [32], for each generated response $\mathbf{y}_i^{(j)}$ relative to the context $\mathbf{x}^{(i)}$ in $\mathcal{Y}^{(i)}$, we evaluate the correctness with respect to a reference answer $\bar{\mathbf{y}}_i$ using an LLM-as-judge approach. The truthfulness label $l^{(i)}$ that indicates the correctness of generated answers $\mathcal{Y}^{(i)}$ is then determined by the majority vote (see Appendix B for further details).

Gaussian Process Classifier. Given a set of generated outputs $\mathcal{Y} := \{\mathbf{y}^{(1)}, \dots, \mathbf{y}^{(N)}\}$ related to a given context \mathbf{x} , the objective is to predict the truthfulness label $l \in \{0, 1\}$ of these generated samples using the semantic consistency vector $\boldsymbol{\lambda} \in \mathbb{R}^N$ defined in equation 9. We do this by computing the label probability

$$p(l \mid \mathcal{Y}, \mathbf{x}, \boldsymbol{\theta}) = p(l \mid \boldsymbol{\lambda}) \quad (10)$$

with a Gaussian Process Classifier (GPC) [71] trained on the dataset $\tilde{\mathcal{D}} := \{\boldsymbol{\lambda}^{(i)}, l^{(i)}\}_{i=1}^M$. In the following, we denote by $\mathbf{l} = [l^{(1)}, \dots, l^{(M)}]^T \in \mathbb{R}^M$ and $\boldsymbol{\Lambda} = [\boldsymbol{\lambda}^{(1)}, \dots, \boldsymbol{\lambda}^{(M)}]^T \in \mathbb{R}^{M \times N}$ the collections of labels and semantic consistency

Table 1. **SGPU** consistently improves AUROC and AUARC while reducing ECE. Evaluation metrics for vision datasets averaged across all LVLM architectures. **Bold** values indicates best performance, underline values indicate the second-best.

Method	CIFAR10				OKVQA				VQARAD				ADVQA				VizWiz				Imagenette			
	AUROC↑	AUARC↑	ECE↓	AUROC↑	AUARC↑	ECE↓	AUROC↑	AUARC↑	ECE↓															
SE	0.823	0.832	0.075	0.763	0.792	0.232	0.691	0.621	0.282	0.673	0.658	0.149	0.785	0.657	0.219	0.604	0.617	0.309						
DSE	0.818	0.832	0.070	0.753	0.787	0.213	0.691	0.599	0.292	0.676	0.659	<u>0.152</u>	0.787	<u>0.651</u>	0.230	0.605	0.614	0.285						
PE	0.812	0.824	0.081	0.737	0.783	0.109	0.705	0.624	0.132	0.672	0.657	<u>0.168</u>	0.764	0.645	0.112	0.624	<u>0.641</u>	0.260						
KLE-Heat	0.827	<u>0.838</u>	0.084	0.731	0.782	0.191	0.644	0.640	0.230	0.688	0.667	0.168	0.746	0.634	0.235	0.589	0.616	0.372						
KLE-Matern	0.832	<u>0.837</u>	<u>0.066</u>	0.762	0.794	0.075	0.684	0.634	0.159	0.700	0.672	0.105	0.765	0.651	<u>0.137</u>	0.590	0.616	0.301						
UMPIRE	0.826	0.800	<u>0.122</u>	<u>0.768</u>	<u>0.777</u>	<u>0.236</u>	<u>0.724</u>	<u>0.622</u>	0.260	0.667	0.621	0.229	0.798	0.616	<u>0.190</u>	0.609	0.600	0.338						
Cos Eigenscore	0.841	0.770	0.127	0.750	0.738	0.123	0.702	0.618	0.201	0.635	0.587	0.201	0.777	0.588	0.156	0.625	0.604	0.336						
Cov Eigenscore	0.787	0.750	0.243	0.685	0.705	0.280	0.695	0.616	0.234	0.620	0.581	0.324	0.711	0.584	0.158	0.769	0.576	0.094						
SGPU (ours)	0.882	0.878	0.036	0.788	0.810	0.072	0.752	0.740	0.210	0.711	0.701	0.173	0.828	0.818	0.356	<u>0.749</u>	0.774	<u>0.199</u>						

vectors, respectively. For a fixed λ , the GPC models $p(l | \lambda)$ as a Bernoulli distribution with parameter $p(l = 1 | \lambda) = s(f(\lambda))$, where $f(\cdot)$ is a latent function and $s : \mathbb{R} \rightarrow [0, 1]$ is a sigmoid function. The latent function $f(\cdot)$ is assumed to follow a Gaussian Process (GP) prior

$$f \sim \mathcal{GP}(m(\lambda), k(\lambda, \lambda')), \quad (11)$$

where $m(\cdot)$ is the mean function and $k(\cdot, \cdot)$ is a kernel function. This implies that the evaluation vector of $f(\cdot)$ on Λ defined as $\mathbf{f} = [f(\lambda_1), \dots, f(\lambda_M)]^T \in \mathbb{R}^M$ is drawn from a multivariate Gaussian distribution $\mathbf{f} \sim \mathcal{N}(\mu, \mathbf{K})$, where $\mu = [m(\lambda_1), \dots, m(\lambda_M)]^T$ and $\mathbf{K}_{ij} = k(\lambda_i, \lambda_j)$. Since neither of the class labels is considered more probable than the others, the prior mean is usually set to zero. The kernel function $k(\cdot, \cdot)$ encodes prior beliefs about the properties of the latent function $f(\cdot)$. The posterior distribution over the latent values \mathbf{f} at the observed Λ is defined as:

$$p(\mathbf{f} | \tilde{\mathcal{D}}) = \frac{1}{p(\tilde{\mathcal{D}})} p(\mathbf{l} | \mathbf{f}) p(\mathbf{f} | \Lambda), \quad (12)$$

where $p(\tilde{\mathcal{D}})$ denotes the marginal likelihood and $p(\mathbf{l} | \mathbf{f}) = \prod_{i=1}^M s(l^{(i)} f(\lambda_i))$ the joint likelihood of the independent Bernoulli variables in \mathbf{l} . The distribution for the latent function value $f = f(\lambda)$ at a new semantic consistency vector λ is obtained by averaging over the posterior distribution

$$p(f | \lambda, \tilde{\mathcal{D}}) = \int p(f | \mathbf{f}, \tilde{\mathcal{D}}) p(\mathbf{f} | \tilde{\mathcal{D}}) d\mathbf{f} \quad (13)$$

and the predictive label probability $p(l | \mathcal{Y}, \mathbf{x}, \theta, \tilde{\mathcal{D}})$ is computed as the expectation:

$$p(l | \mathcal{Y}, \mathbf{x}, \theta, \mathcal{D}) = p(l | \lambda, \tilde{\mathcal{D}}) = \int p(l | f) p(f | \lambda, \tilde{\mathcal{D}}) df,$$

where $p(l | f) = s(l f(\lambda))$. Note that neither the marginal likelihood, nor the posterior itself, or predictions can be computed analytically, so approximations such as Monte-Carlo or Laplace approximations are needed [71].

GPC provides the advantage of direct access to its internal uncertainty estimates (through the predictive standard deviation), requires only a small amount of training data, and is typically well-calibrated. Moreover, it has strong potential to generalize effectively to new or varying inputs. More detailed motivations can be found in Appendix C.

5. Experiments

5.1. Overall Performance Comparison

Datasets and Models. In this section, we evaluate our method across diverse tasks, datasets, and architectures. Our evaluation is conducted on visual question answering (VQA), image classification, and textual Question Answering (QA) tasks. For VQA, we consider four datasets: **ADVQA** [51], **VQARAD** [44], **OKVQA** [62], and **VizWiz** [26]. For image classification, we use **CLIFAR10** [39] and **Imagenette** [30]; while for the QA task, we use **TriviaQA** [36] and **PopQA** [10]. Experiments on vision and VQA tasks are performed with Qwen2.5-VL-3B [83], Qwen2.5-VL-7B [5], llava-mistral-7b [55], idefics2-8b [45]. We conduct experiments with Llama-3.1-8B [83] for QA datasets. Generated answers are embedded with all-MiniLM-L6-v2 [72]. More details on the experimental protocol can be found in Appendix A.1.

Evaluation Metrics. Following previous work [18, 32, 41, 43], we evaluate uncertainty methods using: AUROC [28], AUARC [40], and ECE [24]. AUROC (Area Under the Receiver Operating Curve) is a performance metric for binary classifiers, allowing it to assess whether an uncertainty estimation metric effectively distinguishes between correct and incorrect generations. Higher scores are better, with perfect uncertainty scoring 1 while a random uncertainty measure would score 0.5. AUARC (Area Under the Accuracy-Rejection Curve) measures robustness under selective prediction by averaging accuracy after progressively discarding uncertain samples, where higher AUARC means errors are concentrated in low-confidence regions. ECE (Expected Calibration Error) quantifies how well predicted probabilities align with empirical accuracies, where lower values indicate better calibration. More details on the metrics can be found in Appendix A.3.

Baselines. We compare our proposal with popular uncertainty-based methods: Predictive Entropy (PE) [18, 41], Semantic Entropy (SE) [41], Discrete Semantic En-

tropy (DSE) [18], Kernel Language Entropy (KLE) with a Heat Kernel [67], KLE with a Matern Kernel [67], UMPIRE [43], Cov Eigenscore [11], and Cos Eigenscore [11], a variant of Cov Eigenscore, but based on cosine similarity matrix instead (see 3.2). More details on the baselines can be found in Appendix A.2.

Results and Discussions. Tables 1 & 2 present an overall comparison of uncertainty estimation methods across several datasets and LVLM architectures. Results show that SGPU achieves higher AUROC and AUARC scores while maintaining a lower calibration error (ECE) compared to the baselines. Due to the inherently open-ended nature of free-form NLG, estimating uncertainty is more challenging on VQA tasks than for classification tasks. While baseline methods provide partial improvements in AUROC and AUARC, SGPU significantly outperforms them on these evaluation metrics and maintains a low calibration error (ECE). In particular, SGPU performs significantly better on both Qwen2.5-VL-3B and llava-mistral-7b, where it improves both discrimination and calibration measures. On the medical dataset **VQARAD**, baseline methods show significant degradations, whereas SGPU successfully maintains a better AUROC and a lower ECE. Furthermore, SGPU remains robust and achieves best performance on tasks with adversarial inputs (dataset **ADVQA**). More detailed experiments (LVLM and LLM) can be found in Appendix D.

Detection of Unsafe SGPU Prediction. One motivation for using a GPC is its ability to provide a principled estimate of the predictive standard deviation for each output. This quantity provides a direct characterization of the classifier uncertainty in estimating the underlying semantic uncertainty of the LVLM. By exploiting this information, we can perform a more fine-grained analysis of the GPC predictions and detect cases where the model is inherently uncertain (see Figure 3). This detection can contribute to refining uncertainty predictions with SGPU, as described in Appendix C.

5.2. Transfer Experiments and Generalization

Cross-Model Transferability. An interesting aspect is that the trained SGPU generalizes well across different LVLM architectures. Transfer experiments in Table 3 show that although performance slightly decreases when SGPU is trained on one LVLM and evaluated on another, its predictions remain meaningful. For instance, SGPU trained on Qwen2.5-VL-3B and evaluated on Qwen2.5-VL-7B achieves the same AUROC performance results with only a moderate drop in AUARC. As shown in Appendix A.4, the model transferability remains especially strong on **CIFAR10**, where visual patterns are simpler and more consis-

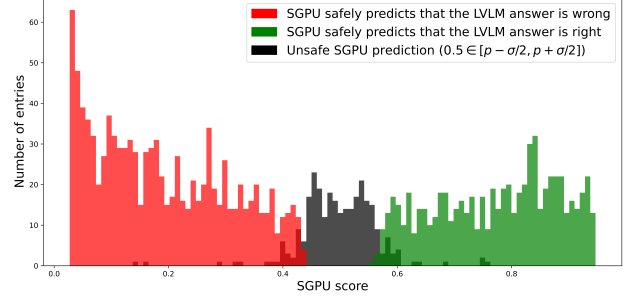


Figure 3. **Detection of Unsafe SGPU Predictions** with llava-mistral-7b on **VIZWIZ**. Unsafe SGPU predictions are defined when $0.5 \in [p - \sigma/2, p + \sigma/2]$, where p is the SGPU score and σ is its associated predicted standard deviation.

tent. Such a result confirms that the semantic consistency vector λ (defined in equation 9) is not entirely tied to a single LVLM architecture and captures stable patterns of semantic consistency across responses. Furthermore, SGPU can be reused across models without requiring full retraining. This suggests that it may serve as a general uncertainty prior for LVLMs, enabling more flexible and efficient adaptation in new domains and across different model families.

Cross-Modality Transferability. Transfer experiments in Table 4 show that although performance slightly decreases when SGPU is trained on one modality and evaluated on another, its predictions remain meaningful. For instance, SGPU trained with Llama-3.1-8B on **TriviaQA** and evaluated on **CIFAR10** with Qwen2.5-VL-3B achieves an AUROC of 0.775. Conversely, when SGPU is trained with Qwen2.5-VL-3B on **CIFAR10** and evaluated on **TriviaQA** with Llama-3.1-8B, it obtains an AUROC of 0.616. This difference likely stems from the fundamentally distinct nature of image classification and textual question-answering tasks, where the types of generated outputs vary significantly. SGPU shows better robustness when transferring between similar tasks across different modalities. For instance, SGPU trained with idefics2-8b on **OKVQA** and evaluated on **TriviaQA** with Llama-3.1-8B achieves an AUROC of 0.818. These results seem to show that SGPU may generalize beyond specific datasets, models or modalities.

5.3. Computational Cost

We compare the inference times of the different methods in Table 5. Our results show that inference times are relatively similar across the various uncertainty estimation methods. Although SGPU uses an additional sentence embedding model to capture semantic consistency across generated answers, this does not significantly increase the overall com-

Table 2. **SGPU consistently improves AUROC and AUARC while reducing ECE.** Evaluation metrics for LVLM architectures averaged across all vision datasets. **Bold** values indicates best performance, underline values indicate the second-best.

Method	Qwen2.5-VL-3B			Qwen2.5-VL-7B			idefics2-8b			llava-mistral-7b		
	AUROC↑	AUARC↑	ECE↓	AUROC↑	AUARC↑	ECE↓	AUROC↑	AUARC↑	ECE↓	AUROC↑	AUARC↑	ECE↓
SE	0.731	0.683	0.165	0.713	0.690	0.244	0.698	0.720	0.250	0.750	0.691	0.186
DSE	0.730	0.681	0.154	0.712	0.687	0.243	0.672	0.716	0.243	0.750	0.678	0.189
PE	0.726	0.682	0.087	0.713	0.692	0.107	0.702	0.724	0.252	0.736	0.685	<u>0.127</u>
ManualHeat	0.726	0.684	0.164	0.715	0.692	0.207	0.688	0.714	0.249	0.687	0.694	0.233
ManualMatern	0.747	<u>0.693</u>	0.145	<u>0.724</u>	<u>0.698</u>	<u>0.097</u>	0.693	0.715	0.230	0.724	<u>0.697</u>	0.089
UMPIRE	0.722	0.618	0.158	0.709	0.658	0.278	0.714	0.727	0.285	<u>0.782</u>	0.688	0.195
Cos Eigenscore	0.699	0.559	0.157	0.714	0.625	0.158	0.736	0.726	0.266	0.737	0.694	0.180
Cov Eigenscore	0.653	0.554	0.196	0.717	0.631	0.177	0.765	0.678	0.229	0.709	0.679	0.288
SGPU (ours)	0.810	0.805	<u>0.102</u>	0.766	0.767	0.080	0.746	0.753	0.242	0.817	0.822	0.274

Table 3. **SGPU generalizes well across different LVLM architectures.** Each row shows the SGPU trained on the outputs of one LVLM and tested on another for the **VQARAD** dataset. **Bold** values indicates best performance, underline values indicate the second-best.

Trained GP	Tested on	AUROC↑	AUARC↑	ECE↓
Qwen2.5-VL-7B	Qwen2.5-VL-7B	0.730	0.710	0.060
Qwen2.5-VL-3B	Qwen2.5-VL-7B	<u>0.730</u>	<u>0.687</u>	<u>0.130</u>
llava-mistral-7b	Qwen2.5-VL-7B	0.729	0.657	0.486
idefics2-8b	Qwen2.5-VL-7B	0.724	0.655	0.255
Qwen2.5-VL-3B	Qwen2.5-VL-3B	0.770	0.770	0.060
Qwen2.5-VL-7B	Qwen2.5-VL-3B	0.700	<u>0.662</u>	<u>0.352</u>
llava-mistral-7b	Qwen2.5-VL-3B	<u>0.727</u>	0.632	0.473
idefics2-8b	Qwen2.5-VL-3B	0.684	0.622	0.345
idefics2-8b	idefics2-8b	0.750	0.664	0.278
Qwen2.5-VL-3B	idefics2-8b	<u>0.636</u>	0.588	0.069
Qwen2.5-VL-7B	idefics2-8b	0.526	0.507	<u>0.176</u>
llava-mistral-7b	idefics2-8b	0.518	<u>0.627</u>	0.443
llava-mistral-7b	llava-mistral-7b	0.758	0.815	0.442
Qwen2.5-VL-3B	llava-mistral-7b	0.754	0.698	<u>0.199</u>
Qwen2.5-VL-7B	llava-mistral-7b	<u>0.754</u>	<u>0.812</u>	0.455
idefics2-8b	llava-mistral-7b	0.721	0.602	0.169

Table 4. **SGPU transfers across modalities.** Each row shows the SGPU trained on one modality and tested on another. **Bold** values indicates best performance.

CIFAR10 / TriviaQA				
Trained on	Tested on	AUROC↑	AUARC↑	ECE↓
CIFAR10 / Qwen2.5-VL-3B	CIFAR10 / Qwen2.5-VL-3B	0.830	0.810	0.010
TriviaQA / Llama-3.1-8B	CIFAR10 / Qwen2.5-VL-3B	0.775	0.745	0.361
TriviaQA / Llama-3.1-8B	TriviaQA / Llama-3.1-8B	0.870	0.867	0.139
CIFAR10 / Qwen2.5-VL-3B	TriviaQA / Llama-3.1-8B	0.616	0.739	0.206
OKVQA / TriviaQA				
Trained on	Tested on	AUROC↑	AUARC↑	ECE↓
OKVQA / idefics2-8b!	OKVQA / idefics2-8b	0.753	0.798	0.150
TriviaQA / Llama-3.1-8B	OKVQA / idefics2-8b	0.679	0.755	0.194
TriviaQA / Llama-3.1-8B!	TriviaQA / Llama-3.1-8B	0.870	0.867	0.139
OKVQA / idefics2-8b!	TriviaQA / Llama-3.1-8B	0.818	0.835	0.237

putation time. The primary computational cost for all methods stems from sampling multiple responses. These observations show that the choice of uncertainty estimation strategy has no significant impact on runtime and confirm that our method is both efficient and practical for real-world inference scenarios.

Table 5. Average inference time over 100 samples on **CIFAR-10**.

Method	Owen2.5-VL-3B	idefics2-8B	llava-mistral-7b
SGPU	0.424 s	3.780 s	11.533 s
Embedding-based	0.526 s	3.976 s	11.420 s
Token-probability based	0.479 s	3.875 s	12.099 s

6. Conclusion

Measuring semantic uncertainty in LVLMs is of critical importance for improving their reliability. In this work, we propose Semantic Gaussian Process Uncertainty (SGPU), a new Bayesian framework for quantifying semantic uncertainty in LVLMs that avoids explicit clustering and operates on the eigenspectrum of answer embeddings.

Our approach provides three main advantages. First, SGPU achieves strong and often state-of-the-art performance across models and datasets on standard uncertainty-evaluation metrics such as AUROC, AUARC, and ECE, with particularly strong results on AUROC. Second, SGPU works in a fully black-box setting: it does not require access to internal model features, embeddings, or token-level probabilities. This makes it applicable to most real-world LVLMs where internal access is not available. Third, by using a Gaussian Process Classifier, SGPU can quantify its own uncertainty while predicting the uncertainty of the LVLM. This extra layer of confidence estimation makes the final predictions more stable and reliable. Overall, SGPU offers a simple, scalable, and robust way to measure uncertainty in modern LVLMs, in both white-box and black-box scenarios.

Limitations. A current limitation of SGPU relies on the use of multiple generations to compute semantic uncertainty, which increases computational cost. Nevertheless, our results demonstrate the potential of classifiers trained on similarity-matrix representations of model outputs. Future work may further explore this direction, develop more efficient sampling strategies, and investigate extensions to larger-scale or real-time settings.

References

[1] Samir Abdaljalil, Hasan Kurban, Panchit Sharma, Erchin Serpedin, and Rachad Atat. Sindex: Semantic inconsistency index for hallucination detection in llms. *arXiv preprint arXiv:2503.05980*, 2025. 2, 3, 5

[2] Moloud Abdar, Farhad Pourpanah, Sadiq Hussain, Dana Rezazadegan, Li Liu, Mohammad Ghavamzadeh, Paul Fieguth, Xiaochun Cao, Abbas Khosravi, U. Rajendra Acharya, Vladimir Makarenkov, and Saeid Nahavandi. A review of uncertainty quantification in deep learning: Techniques, applications and challenges. *IF*, 2021. 2, 3

[3] Lukas Aichberger, Kajetan Schweighofer, and Sepp Hochreiter. Rethinking uncertainty estimation in natural language generation. *arXiv preprint arXiv:2412.15176*, 2024. 2

[4] Amos Azaria and Tom Mitchell. The internal state of an LLM knows when it's lying. In *EMNLP*, 2023. 2, 3, 4

[5] Shuai Bai, Keqin Chen, Xuejing Liu, Jialin Wang, Wenbin Ge, Sibo Song, Kai Dang, Peng Wang, Shijie Wang, Jun Tang, et al. Qwen2. 5-vl technical report. *arXiv preprint arXiv:2502.13923*, 2025. 6

[6] Neil Band, Tim G. J. Rudner, Qixuan Feng, Angelos Filos, Zachary Nado, Mike Dusenberry, Ghassen Jerfel, Dustin Tran, and Yarin Gal. Benchmarking bayesian deep learning on diabetic retinopathy detection tasks. In *NeurIPS Datasets and Benchmarks*, 2021. 5

[7] Anton Baumann, Rui Li, Marcus Klasson, Santeri Menta, Shyamgopal Karthik, Zeynep Akata, Arno Solin, and Martin Trapp. Post-hoc probabilistic vision-language models. *arXiv preprint arXiv:2412.06014*, 2024. 3

[8] Jakub Binkowski, Denis Janiak, Albert Sawczyn, Bogdan Gabrys, and Tomasz Jan Kajdanowicz. Hallucination detection in LLMs using spectral features of attention maps. In *EMNLP*, 2025. 3

[9] Charles Blundell, Julien Cornebise, Koray Kavukcuoglu, and Daan Wierstra. Weight uncertainty in neural network. In *ICML*, 2015. 2

[10] Yapei Chang, Hangfeng He, and Dan Roth. Popqa: A question answering benchmark for evaluating the factual consistency of language models. In *NAACL*, 2023. 6, 1, 3

[11] Chao Chen, Kai Liu, Ze Chen, Yi Gu, Yue Wu, Mingyuan Tao, Zhihang Fu, and Jieping Ye. INSIDE: LLMs' internal states retain the power of hallucination detection. In *ICLR*, 2024. 2, 4, 5, 7, 1

[12] Tiejin Chen, Xiaou Liu, Longchao Da, Jia Chen, Vagelis Papalexakis, and Hua Wei. Uncertainty quantification of large language models through multi-dimensional responses. *arXiv preprint arXiv:2502.16820*, 2025. 2

[13] Roi Cohen, May Hamri, Mor Geva, and Amir Globerson. LM vs LM: Detecting factual errors via cross examination. In *EMNLP*, 2023. 3

[14] Roi Cohen, Konstantin Dobler, Eden Biran, and Gerard de Melo. I don't know: Explicit modeling of uncertainty with an [idk] token. In *NeurIPS*, 2024. 3

[15] Erik Daxberger, Agustinus Kristiadi, Alexander Immer, Runa Eschenhagen, Matthias Bauer, and Philipp Hennig. Laplace redux-effortless bayesian deep learning. In *NeurIPS*, 2021. 3

[16] Jia Deng, Wei Dong, Richard Socher, Li-Jia Li, Kai Li, and Li Fei-Fei. Imagenet: A large-scale hierarchical image database. In *CVPR*, 2009. 1

[17] Davide Ettori, Nastaran Darabi, Sina Tayebati, Ranganath Krishnan, Mahesh Subedar, Omesh Tickoo, and Amit Ranjan Trivedi. Eigentrack: Spectral activation feature tracking for hallucination and out-of-distribution detection in llms and vlms. *arXiv preprint arXiv:2509.15735*, 2025. 3, 4

[18] Sebastian Farquhar, Jannik Kossen, Lorenz Kuhn, and Yarin Gal. Detecting hallucinations in large language models using semantic entropy. *Nature*, 2024. 2, 3, 4, 5, 6, 7, 1

[19] Gianni Franchi, Andrei Bursuc, Emanuel Aldea, Séverine Dubuisson, and Isabelle Bloch. Tradi: Tracking deep neural network weight distributions. 2020. 3

[20] Firas Gabetni, Giuseppe Curci, Andrea Pilzer, Subhankar Roy, Elisa Ricci, and Gianni Franchi. Ensembling pruned attention heads for uncertainty-aware efficient transformers. *arXiv preprint arXiv:2510.18358*, 2025. 3

[21] Yarin Gal and Zoubin Ghahramani. Dropout as a bayesian approximation: Representing model uncertainty in deep learning. In *ICML*, 2016. 2

[22] Xiang Gao, Jiaxin Zhang, Lalla Mouatadid, and Kamalika Das. SPUQ: Perturbation-based uncertainty quantification for large language models. In *EACL*, 2024. 3

[23] Yashvir S Grewal, Edwin V Bonilla, and Thang D Bui. Improving uncertainty quantification in large language models via semantic embeddings. *arXiv preprint arXiv:2410.22685*, 2024. 2, 3

[24] Chuan Guo, Geoff Pleiss, Yu Sun, and Kilian Q Weinberger. On calibration of modern neural networks. In *ICML*, 2017. 6, 1

[25] Daya Guo, Dejian Yang, Haowei Zhang, Junxiao Song, Peiyi Wang, Qihao Zhu, Runxin Xu, Ruoyu Zhang, Shirong Ma, Xiao Bi, et al. Deepseek-r1 incentivizes reasoning in llms through reinforcement learning. *Nature*, 2025. 1

[26] Danna Gurari, Qing Li, Abigale J Stangl, Anhong Guo, Chi Lin, Kristen Grauman, Jiebo Luo, and Jeffrey P Bigham. Vizwiz grand challenge: Answering visual questions from blind people. In *CVPR*, 2018. 6, 1

[27] Pengcheng He, Xiaodong Liu, Jianfeng Gao, and Weizhu Chen. {DEBERTA}: {DECODING}-{enhanced} {bert} {with} {disentangled} {attention}. In *International Conference on Learning Representations*, 2021. 2

[28] Dan Hendrycks and Kevin Gimpel. A baseline for detecting misclassified and out-of-distribution examples in neural networks. In *ICLR*, 2017. 6, 1

[29] Jose Miguel Hernandez-Lobato and Ryan Adams. Probabilistic backpropagation for scalable learning of bayesian neural networks. In *ICML*, 2015. 2

[30] Jeremy Howard. Imagenette: A smaller subset of 10 easily classified classes from imagenet. <https://github.com/fastai/imagenette>, 2019. 6

[31] Lei Huang, Weijiang Yu, Weitao Ma, Weihong Zhong, Zhangyin Feng, Haotian Wang, Qianglong Chen, Weihua Peng, Xiaocheng Feng, Bing Qin, and Ting Liu. A survey on hallucination in large language models: Principles, taxonomy, challenges, and open questions. *TIS*, 2025. 1

[32] Denis Janiak, Jakub Binkowski, Albert Sawczyn, Bogdan Gabrys, Ravid Shwartz-Ziv, and Tomasz Jan Kajdanowicz. The illusion of progress: Re-evaluating hallucination detection in LLMs. In *EMNLP*, 2025. 2, 4, 5, 6

[33] Ziwei Ji, Nayeon Lee, Rita Frieske, Tiezheng Yu, Dan Su, Yan Xu, Etsuko Ishii, Ye Jin Bang, Andrea Madotto, and Pascale Fung. Survey of hallucination in natural language generation. *CS*, 2023. 1

[34] Ziwei Ji, Lei Yu, Yeskendir Koishkenov, Yejin Bang, Anthony Hartshorn, Alan Schelten, Cheng Zhang, Pascale Fung, and Nicola Cancedda. Calibrating verbal uncertainty as a linear feature to reduce hallucinations. *arXiv preprint arXiv:2503.14477*, 2025. 3

[35] Minsuh Joo and Hyunsoo Cho. Cleanse: Uncertainty estimation approach using clustering-based semantic consistency in LLMs. In *ACL Workshops*, 2025. 2, 3

[36] Mandar Joshi, Eunsol Choi, Daniel S. Weld, and Luke Zettlemoyer. Triviaqa: A large scale distantly supervised challenge dataset for reading comprehension. In *ACL*, 2017. 6, 1, 3

[37] Saurav Kadavath, Tom Conerly, Amanda Askell, Tom Henighan, Dawn Drain, Ethan Perez, Nicholas Schiefer, Zac Hatfield-Dodds, Nova DasSarma, Eli Tran-Johnson, et al. Language models (mostly) know what they know. *arXiv preprint arXiv:2207.05221*, 2022. 3, 1

[38] Jannik Kossen, Jiatong Han, Muhammed Razzak, Lisa Schut, Shreshth Malik, and Yarin Gal. Semantic entropy probes: Robust and cheap hallucination detection in llms. *arXiv preprint arXiv:2406.15927*, 2024. 2

[39] Alex Krizhevsky, Geoffrey Hinton, et al. Learning multiple layers of features from tiny images. 2009. 6, 1

[40] Lorenz Kuhn, Yarin Gal, and Sebastian Farquhar. Semantic uncertainty: Linguistic invariances for uncertainty estimation in natural language generation. In *ICLR*, 2023. 6, 1

[41] Lorenz Kuhn, Yarin Gal, and Sebastian Farquhar. Semantic uncertainty: Linguistic invariances for uncertainty estimation in natural language generation. In *ICLR*, 2023. 2, 3, 4, 5, 6, 1

[42] Balaji Lakshminarayanan, Alexander Pritzel, and Charles Blundell. Simple and scalable predictive uncertainty estimation using deep ensembles. In *NeurIPS*, 2017. 2, 3

[43] Gregory Kang Ruey Lau, Hieu Dao, Nicole Kan Hui Lin, and Bryan Kian Hsiang Low. Uncertainty quantification for multimodal large language models with coherence-adjusted semantic volume, 2025. 2, 3, 4, 5, 6, 7, 1

[44] Jason J Lau, Soumya Gayen, Asma Ben Abacha, and Dina Demner-Fushman. A dataset of clinically generated visual questions and answers about radiology images. *Scientific data*, 2018. 6, 1

[45] Hugo Laurençon, Léo Tronchon, Matthieu Cord, and Victor Sanh. What matters when building vision-language models? In *NeurIPS*, 2024. 6

[46] Olivier Laurent, Adrien Lafage, Enzo Tartaglione, Geoffrey Daniel, Jean-Marc Martinez, Andrei Bursuc, and Gianni Franchi. Packed-ensembles for efficient uncertainty estimation. *arXiv preprint arXiv:2210.09184*, 2022. 3

[47] Olivier Laurent, Emanuel Aldea, and Gianni Franchi. A symmetry-aware exploration of bayesian neural network posteriors. *arXiv preprint arXiv:2310.08287*, 2023. 2

[48] Sungjae Lee, Hoyoung Kim, Jeongyeon Hwang, Eunhyeok Park, and Jungseul Ok. Efficient latent semantic clustering for scaling test-time computation of llms, 2025. 2, 3

[49] Patrick Lewis, Ethan Perez, Aleksandra Piktus, Fabio Petroni, Vladimir Karpukhin, Naman Goyal, Heinrich Küttler, Mike Lewis, Wen-tau Yih, Tim Rocktäschel, Sebastian Riedel, and Douwe Kiela. Retrieval-augmented generation for knowledge-intensive nlp tasks. In *NeurIPS*, 2020. 5

[50] Kenneth Li, Oam Patel, Fernanda Viégas, Hanspeter Pfister, and Martin Wattenberg. Inference-time intervention: Eliciting truthful answers from a language model. In *NeurIPS*, 2023. 3

[51] Linjie Li, Jie Lei, Zhe Gan, and Jingjing Liu. Adversarial vqa: A new benchmark for evaluating the robustness of vqa models. In *ICCV*, 2021. 6, 1

[52] Xiaomin Li, Zhou Yu, Ziji Zhang, Yingying Zhuang, Swair Shah, Narayanan Sadagopan, and Anurag Beniwal. Semantic volume: Quantifying and detecting both external and internal uncertainty in llms. *arXiv preprint arXiv:2502.21239*, 2025. 3, 4, 1

[53] Stephanie Lin, Jacob Hilton, and Owain Evans. Teaching models to express their uncertainty in words. *TMLR*, 2022. 3

[54] Zhen Lin, Shubhendu Trivedi, and Jimeng Sun. Generating with confidence: Uncertainty quantification for black-box large language models. *TMLR*, 2024. 3, 1

[55] Haotian Liu, Chunyuan Li, Yuheng Li, and Yong Jae Lee. Improved baselines with visual instruction tuning. In *CVPR*, 2024. 6

[56] Hanchao Liu, Wenyuan Xue, Yifei Chen, Dapeng Chen, Xiutian Zhao, Ke Wang, Liping Hou, Rongjun Li, and Wei Peng. A survey on hallucination in large vision-language models. *arXiv preprint arXiv:2402.00253*, 2024. 1

[57] David JC MacKay. Probable networks and plausible predictions-a review of practical bayesian methods for supervised neural networks. *Network: computation in neural systems*, 1995. 2

[58] David John Cameron Mackay. *Bayesian methods for adaptive models*. CalTech, 1992. 2

[59] Wesley J Maddox, Pavel Izmailov, Timur Garipov, Dmitry P Vetrov, and Andrew Gordon Wilson. A simple baseline for bayesian uncertainty in deep learning. *NeurIPS*, 2019. 3

[60] Andrey Malinin and Mark Gales. Uncertainty estimation in autoregressive structured prediction. In *ICLR*, 2021. 2, 3

[61] Potsawee Manakul, Adian Liusie, and Mark Gales. Self-CheckGPT: Zero-resource black-box hallucination detection for generative large language models. In *EMNLP*, 2023. 3, 5

[62] Kenneth Marino, Mohammad Rastegari, Ali Farhadi, and Roozbeh Mottaghi. Ok-vqa: A visual question answering benchmark requiring external knowledge. In *CVPR*, 2019. 6, 1

[63] Kevin P Murphy. *Machine learning: a probabilistic perspective*. MIT press, 2012. 2

[64] Kenton Murray and David Chiang. Correcting length bias in neural machine translation. In *MT*, 2018. 3

[65] Radford M Neal. *Bayesian learning for neural networks*. Springer Science & Business Media, 2012. 2

[66] Dang Nguyen, Ali Payani, and Baharan Mirzasoleiman. Beyond semantic entropy: Boosting LLM uncertainty quantification with pairwise semantic similarity. In *ACL*, 2025. 2

[67] Alexander Nikitin, Jannik Kossen, Yarin Gal, and Pekka Marttinen. Kernel language entropy: Fine-grained uncertainty quantification for llms from semantic similarities. In *NeurIPS*, 2024. 2, 3, 7, 1

[68] Alexander Novikov, Ngan Vū, Marvin Eisenberger, Emiel Dupont, Po-Sen Huang, Adam Zsolt Wagner, Sergey Shirobokov, Borislav Kozlovskii, Francisco JR Ruiz, Abbas Mehrabian, et al. Alphaevolve: A coding agent for scientific and algorithmic discovery. *arXiv preprint arXiv:2506.13131*, 2025. 1

[69] Hadas Orgad, Michael Toker, Zorik Gekhman, Roi Reichart, Idan Szpektor, Hadas Kotek, and Yonatan Belinkov. LLMs know more than they show: On the intrinsic representation of LLM hallucinations. In *ICLR*, 2025. 2, 3, 4

[70] Xin Qiu and Risto Miikkulainen. Semantic density: Uncertainty quantification for large language models through confidence measurement in semantic space. In *NeurIPS*, 2024. 3

[71] Carl Edward Rasmussen and Christopher K. I. Williams. *Gaussian Processes for Machine Learning*. The MIT Press, 2005. 5, 6

[72] Nils Reimers and Iryna Gurevych. Sentence-bert: Sentence embeddings using siamese bert-networks. *arXiv preprint arXiv:1908.10084*, 2019. 5, 6, 2

[73] Jie Ren, Jiaming Luo, Yao Zhao, Kundan Krishna, Mohammad Saleh, Balaji Lakshminarayanan, and Peter J Liu. Out-of-distribution detection and selective generation for conditional language models. In *ICLR*, 2023. 3

[74] Hippolyt Ritter, Aleksandar Botev, and David Barber. A scalable laplace approximation for neural networks. In *ICLR*, 2018. 3

[75] Bernhard Schölkopf and Alexander J Smola. *Learning with kernels: support vector machines, regularization, optimization, and beyond*. MIT press, 2002. 5

[76] Ravid Shwartz-Ziv, Randall Balestrieri, Kenji Kawaguchi, Tim G. J. Rudner, and Yann LeCun. An information theory perspective on variance-invariance-covariance regularization. In *NeurIPS*, 2023. 4

[77] Oscar Skean, Md Rifat Arefin, Dan Zhao, Niket Nikul Patel, Jalal Naghiyev, Yann LeCun, and Ravid Shwartz-Ziv. Layer by layer: Uncovering hidden representations in language models. In *ICML*, 2025. 5

[78] Gaurang Sriramanan, Siddhant Bharti, Vinu Sankar Sadasivan, Shoumik Saha, Priyatham Kattakinda, and Soheil Feizi. Llm-check: Investigating detection of hallucinations in large language models. In *NeurIPS*, 2024. 2, 4, 5

[79] Gemini Team. Gemini 1.5: Unlocking multimodal understanding across millions of tokens of context, 2024. 1

[80] Meta team. The llama 3 herd of models, 2024. 3

[81] OpenAI team. Gpt-4 technical report, 2024. 1

[82] OpenAI team. gpt-oss-120b and gpt-oss-20b model card, 2025. 1

[83] Haoran Wei, Yaofeng Sun, and Yukun Li. Deepseek-ocr: Contexts optical compression. *arXiv preprint arXiv:2510.18234*, 2025. 6

[84] Yeming Wen, Dustin Tran, and Jimmy Ba. Batchensemble: an alternative approach to efficient ensemble and lifelong learning, 2020. 3

[85] Christopher KI Williams and Carl Edward Rasmussen. *Gaussian processes for machine learning*. MIT press Cambridge, MA, 2006. 2

[86] Thomas Wolf, Lysandre Debut, Victor Sanh, Julien Chau-mond, Clement Delangue, Anthony Moi, Pierrick Cistac, Tim Rault, Rémi Louf, Morgan Funtowicz, Joe Davison, Sam Shleifer, Patrick von Platen, Clara Ma, Yacine Jernite, Julien Plu, Canwen Xu, Teven Le Scao, Sylvain Gugger, Mariama Drame, Quentin Lhoest, and Alexander M. Rush. Transformers: State-of-the-art natural language processing. In *Proceedings of the 2020 Conference on Empirical Methods in Natural Language Processing: System Demonstrations*, pages 38–45, Online, 2020. Association for Computational Linguistics. 1

[87] Tunyu Zhang, Haizhou Shi, Yibin Wang, Hengyi Wang, Xiaoxiao He, Zhiwei Li, Haoxian Chen, Ligong Han, Kai Xu, Huan Zhang, et al. Token-level uncertainty estimation for large language model reasoning. *arXiv preprint arXiv:2505.11737*, 2025. 3

[88] Zhanghao Zhouyin and Ding Liu. Understanding neural networks with logarithm determinant entropy estimator. *arXiv preprint arXiv:2105.03705*, 2021. 4

[89] Zhanghao Zhouyin and Ding Liu. Understanding neural networks with logarithm determinant entropy estimator. *Neuro-computing*, 2025. 4

Improving Semantic Uncertainty Quantification in LVLMs with Semantic Gaussian Processes

Supplementary Material

A. Experimental Settings

In this section, we provide additional details about the experimental protocol used in Section 5.

A.1. Datasets

We evaluate SGPU on visual question answering (VQA), image classification, and textual Question Answering (QA) tasks.

Visual Question-Answering. For VQA, we consider four datasets: **ADVQA** [51], which consists of a training set of 6,000 samples and a test set of 2,000 samples both drawn from the original training set; **VQARAD** [44], which consists of a training set of 2,000 samples from the original training set and a test set of 500 samples from the original test set; **OKVQA** [62], which consists of a training set of 9,000 samples drawn from the original training set and a test set of 5,000 samples drawn from the original validation set; and **VizWiz** [26], which consists of a training set of 10,000 samples and a test set of 2,000 samples both drawn from the original training set.

Image Classification. For image classification, we use the **CIFAR-10** [39] and **Imagenette** [16] datasets, each split into a training set of 10,000 samples drawn from the original training data and a test set of 5,000 samples taken from the original validation set.

Question-Answering. For text-based QA, we use the **TriviaQA** [36] and **PopQA** [10] datasets, each split into a training set of 10,000 samples drawn from the original training data and a test set of 1,000 samples taken from the original test set.

A.2. Baselines

We compare SGPU with popular uncertainty-based methods.

Token-based Measures. For token-based measures, we consider the following: **Predictive Entropy (PE)** [18, 37, 54] defined in equation 3; **Semantic Entropy (SE)** [18, 41] defined in equation 5; **Discrete Semantic Entropy (DSE)** [18, 41] defined in equation 6; **Kernel Language Entropy (KLE)** [67], which captures semantic similarities by applying a distance measure in the space of the generated answers. In particular, KLE uses an external NLI model to

construct a semantic graph over the generated responses and then computes the von Neumann entropy of a graph kernel formed by combination of the graph Laplacian with a pre-defined kernel.

Latent-based Measures. We also examine semantic uncertainty measures that exploit dense semantic information retained within the internal states of LVLMs. In particular, we consider: **Cos Eigenscore** [43, 52] and **Cov Eigenscore** [11], which are semantic volume-based measures (see equation 7) that compute the volume with the cosine similarity matrix and the empirical covariance matrix of the feature representations, respectively. We further include **UMPIRE** [43], which combines the semantic volume with the probabilities of generated answers.

A.3. Metrics

AUROC (Area Under the ROC Curve). We assign a probability score to each example for belonging to the positive class (positive reflects that the LVLM is certain about its answer). AUROC [28] measures how well these scores rank true positives above true negatives. It is the chance that a randomly chosen positive example receives a higher score than a randomly chosen negative one. Higher AUROC means better class separation.

AUARC (Area Under Accuracy–Retention Curve). Each prediction has an associated uncertainty. We sort predictions from most confident to least confident and progressively discard (abstain on) the most uncertain ones. For every retention level (fraction kept), we compute the accuracy on the retained subset. AUARC [40] summarizes how accuracy improves as we keep only confident predictions. Higher AUARC means uncertainty is useful for selective prediction.

ECE (Expected Calibration Error). Each prediction has a confidence value. We group predictions into bins of similar confidence and compare, within each bin, the average confidence to the actual fraction that is correct. ECE [24] is the average mismatch across bins. Lower ECE means the reported confidences align well with true correctness (the model is better calibrated).

A.4. Experimental Settings

For our experiments, we use the Transformer library [86]. For each sample, we sample 20 candidate answers using

`top_p=0.9, top_k=50, and temperature=1.0`. All models perform inference in `torch.float16` precision on NVIDIA H100 NVL GPUs. We use all-MiniLM-L6-v2 [72] for sentence embedding with mean pooling and use the Deberta-large for NLI [27].

B. Truthfulness Label Generation

Given an input $x^{(i)}$, the LVLM generates a set of 20 candidate answers denoted as $\mathcal{Y}^{(i)} := \{\mathbf{y}_i^{(j)}\}_{j=1}^{20}$. Following recommendations in [32], for each generated response $\mathbf{y}_i^{(j)}$ relative to the context $x^{(i)}$ in $\mathcal{Y}^{(i)}$, we evaluate the correctness $l^{(i)}$ with respect to a reference answer \bar{y}_i using an LLM-as-judge approach. In particular, we use Llama-3.1-8B to compare each output $\mathbf{y}_i^{(j)}$ with the reference answer \bar{y}_i and assigns a binary score $l_j^{(i)} \in \{0, 1\}$ to indicate whether $\mathbf{y}_i^{(j)}$ is correct. The prompt we used is depicted in box B. The most frequent label among $\{l_1^{(i)}, \dots, l_{20}^{(i)}\}$ is then selected to define the overall truthfulness label $l^{(i)}$ that indicates the correctness of generated answers $\mathcal{Y}^{(i)}$.

Prompt for Evaluating Correctness of Generated Answers

We are assessing the quality of answers to the following question: [question].
 The expected answer is: [correct answers].
 The proposed answer is: [predicted answer].
 Within the context of the question, does the proposed answer mean the same as the expected answer?
 Respond only with yes or no.
 Response:

Figures A.5 and A.6 illustrate examples of our generation and labeling pipeline on OKVQA using Qwen2.5-VL-3B. In Figure A.5, after generating an answer, the LLM-as-judge approach classifies the LVLM prediction as correct and assigns it the label 1. In contrast, in Figure A.6, the predicted answer is judged incorrect and thus assigned the label 0.

C. Motivations Behind the Gaussian Process

As mentioned in Section 4, the use of a Gaussian Process Classifier (GPC) is motivated by its ability to provide direct access to internal uncertainty estimates (through the predictive standard deviation), its efficiency with limited training data, and its generally good calibration. Moreover, the GPC shows strong potential to generalize effectively to new or varying inputs.

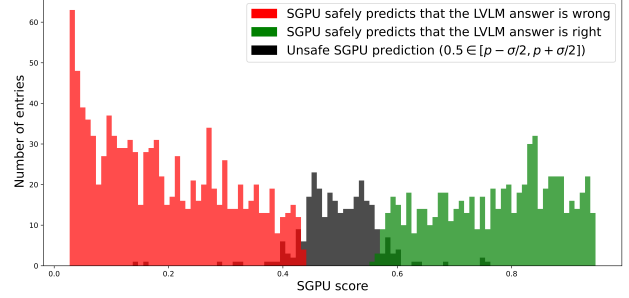


Figure A.4. **Detection of Unsafe SGPU Predictions** with llava-mistral-7b on **VIZWIZ**. Unsafe SGPU predictions are defined when $0.5 \in [p - \sigma/2, p + \sigma/2]$, where p is the SGPU score and σ is its associated predicted standard deviation.

C.1. SGPU Internal Uncertainty

When using a GPC, each prediction provides two key values: the class probability and the corresponding predictive standard deviation. In particular, in the SGPU framework, the GPC returns the probability that the generated answers are correct. Predicted probabilities close to 1 or 0 indicate thus high confidence, whereas values near 0.5 correspond to a region of uncertainty. A naïve way to exclude uncertain predictions would be to discard samples with probabilities close to 0.5 based on an arbitrary threshold. In other words, we could exclude entries for which the associated probability p follows: $\max(p, 1 - p) < 0.5 + \epsilon$, with ϵ being completely randomly chosen.

However, the SGPU offers a more principled approach to quantifying predictive uncertainty through the use of a GPC with the predictive standard deviation, which captures the internal uncertainty for each prediction. Using the predictive standard deviation, we flag a prediction as *unsafe* if adding or subtracting half of the predictive standard deviation to the predicted probability changes the resulting class label. Figure A.4 depicts this classification on **VizWiz** with llava-mistral-7b, with unsafe predictions shown in black. To verify that these predictions are indeed unreliable, we compute the AUROC (using the same setup as in the main experiment) before and after removing the unsafe entries. As expected, the AUROC increases from 0.828 to 0.853 after filtering these entries, confirming that our criterion effectively identifies uncertain predictions.

C.2. SGPU Training Requirements.

Unlike training-free UQ approaches, SGPU requires training and is therefore more computationally expensive. However, Gaussian Processes are known to perform well even with limited training data. To illustrate this, we conducted experiments using progressively smaller subsets of the training data and report the resulting metrics in Ta-

Table A.6. **SGPU requires only a few training samples.** Evaluation of SGPU with varying training dataset sizes. SGPU n denotes SGPU trained with only n samples. **Bold** values indicate best performance.

Dataset	Method	llava-mistral-7b		
		AUROC	AUARC	ECE
VizWiz	SE	0.790	0.671	0.254
	DSE	0.791	0.666	0.276
	Regular	0.755	0.650	0.046
	KLE-Heat	0.726	0.632	0.218
	KLE-Matern	0.764	0.657	0.046
	UMPIRE	0.789	0.627	0.182
	Cos Eigenscore	0.760	0.580	0.100
	Cov Eigenscore	0.701	0.546	0.092
	SGPU (ours)	0.828	0.814	0.319
	SGPU 1000	0.816	0.804	0.293
	SGPU 500	0.811	0.796	0.292
	SGPU 200	0.800	0.780	0.293
	SGPU 100	0.773	0.759	0.314

ble A.6. The results show that even with a very small number of training samples, SGPU achieves competitive performance. In particular, with only 200 training instances, it outperforms existing state-of-the-art methods. These findings confirm that our uncertainty estimation framework remains effective and robust even under constrained data availability.

D. Additional Experiments

D.1. Additional Experiments on LLM

We also evaluate SGPU on text-only tasks and LLM with Llama-3.1-8B-Instruct [80], using the same experimental setup as in the multimodal experiments. In particular, we conduct our experiments on two question-answering (QA) benchmarks: TriviaQA [36] and PopQA [10]. As shown in Table A.7, our method generalizes effectively to text-only tasks, achieving the highest AUROC and AUARC scores on both datasets.

D.2. Transferability

As discussed previously, an appealing property of our approach is that the trained SGPU generalizes well across different LVLM architectures. For VQA tasks, Table 3 shows substantial cross-model transfer: a model trained using outputs from one LVLM can be applied effectively to another with only a small loss in performance. This effect is even more pronounced for image classification. As illustrated in Table A.8, we observe almost no degradation in AUROC and AUARC when the training and testing data are generated from different models. These results indicate that the distribution of eigenvalues does not depend strongly on a specific LVLM architecture, and that our method exhibits robust generalization across models.

Table A.7. **SGPU consistently improves AUROC and AUARC while reducing ECE.** Comparison across QA datasets, metrics, and LLM architectures. **Bold** values indicate best performance.

Dataset	Method	Llama-3.1-8B		
		AUROC	AUARC	ECE
TRIVIA-QA	SE	0.821	0.836	0.255
	DSE	0.828	0.838	0.281
	Regular	0.752	0.819	0.060
	KLE-Heat	0.844	0.847	0.105
	KLE-Matern	0.860	0.851	0.078
	UMPIRE	0.839	0.821	0.310
	Cos Eigenscore	0.833	0.786	0.080
	Cov Eigenscore	0.724	0.740	0.240
	SGPU (ours)	0.870	0.867	0.139
	SE	0.739	0.618	0.130
	DSE	0.734	0.623	0.159
	Regular	0.678	0.646	0.334
POP-QA	ManualHeat	0.664	0.646	0.455
	ManualMatern	0.705	0.626	0.656
	UMPIRE	0.871	0.570	0.050
	Cos Eigenscore	0.853	0.846	0.132
	Cov Eigenscore	0.784	0.753	0.114
	SGPU (ours)	0.908	0.902	0.420

Table A.8. **SGPU generalizes well across different LVLM architectures.** Each row shows the SGPU trained on the outputs of one LVLM and tested on another for the CIFAR dataset. **Bold** values indicate best performance.

Trained GP	Tested on	AUROC	AUARC	ECE
Qwen2.5-VL-7B	Qwen2.5-VL-7B	0.887	0.885	0.007
Qwen2.5-VL-3B	Qwen2.5-VL-7B	0.851	0.854	0.154
llava-mistral-7b	Qwen2.5-VL-7B	0.885	0.876	0.175
idefics2-8b	Qwen2.5-VL-7B	0.882	0.866	0.302
Qwen2.5-VL-3B	Qwen2.5-VL-3B	0.830	0.810	0.010
Qwen2.5-VL-7B	Qwen2.5-VL-3B	0.821	0.771	0.436
llava-mistral-7b	Qwen2.5-VL-3B	0.822	0.792	0.405
idefics2-8b	Qwen2.5-VL-3B	0.763	0.676	0.479
idefics2-8b	idefics2-8b	0.867	0.892	0.013
Qwen2.5-VL-3B	idefics2-8b	0.799	0.863	0.124
Qwen2.5-VL-7B	idefics2-8b	0.862	0.888	0.069
llava-mistral-7b	idefics2-8b	0.862	0.883	0.109
llava-mistral-7b	llava-mistral-7b	0.945	0.925	0.115
Qwen2.5-VL-3B	llava-mistral-7b	0.923	0.917	0.232
Qwen2.5-VL-7B	llava-mistral-7b	0.944	0.919	0.202
idefics2-8b	llava-mistral-7b	0.941	0.802	0.357

D.3. LVLM Complete Results

Table A.9 presents a summary of all results discussed in Section 5.

Table A.9. **SGPU** consistently improves AUROC and AUARC while reducing ECE. Comparison across vision datasets, metrics, and LViM backbones. **Bold** values indicates best performance, underline values indicate the second-best.

Dataset	Method	Qwen2.5-VL-3B			Qwen2.5-VL-7B			idefics2-8b			llava-mistral-7b			Mean		
		AUROC	AUARC	ECE	AUROC	AUARC	ECE	AUROC	AUARC	ECE	AUROC	AUARC	ECE	AUROC	AUARC	ECE
CIFAR10	SE	0.741	0.712	0.066	0.808	0.832	0.102	0.841	0.876	0.105	0.904	0.909	0.026	0.823	0.832	0.075
	DSE	0.750	0.716	0.101	0.802	0.829	0.062	0.837	0.874	<u>0.096</u>	0.903	<u>0.909</u>	<u>0.022</u>	0.818	0.832	0.070
	PE	0.732	0.700	0.110	0.782	0.814	0.072	0.836	<u>0.876</u>	0.099	0.898	0.907	0.043	0.812	0.824	0.081
	KLE-Heat	<u>0.796</u>	<u>0.742</u>	0.069	0.806	0.832	0.089	0.823	0.873	0.120	0.882	0.905	0.058	0.827	<u>0.838</u>	0.084
	KLE-Matern	0.787	0.736	0.096	0.809	<u>0.832</u>	<u>0.056</u>	0.832	0.873	0.098	0.899	0.908	0.015	0.832	0.837	<u>0.066</u>
	UMPIRE	0.724	0.629	0.097	0.793	0.798	0.187	0.856	0.873	0.144	<u>0.929</u>	0.901	0.060	0.826	0.800	0.122
	Cos Eigenscore	0.744	0.559	0.190	0.840	0.780	0.100	0.871	0.867	0.123	0.907	0.874	0.093	<u>0.841</u>	0.770	0.127
	Cov Eigenscore	0.660	0.510	0.058	0.819	0.778	0.209	0.841	0.863	0.430	0.826	0.849	0.275	0.787	0.750	0.243
SGPU (ours)		0.830	0.810	0.010	0.887	0.885	0.007	<u>0.867</u>	0.892	0.013	0.945	0.925	0.115	0.882	0.878	0.036
OKVQA	SE	0.778	0.811	0.181	0.739	0.754	0.387	0.734	0.787	0.156	<u>0.800</u>	<u>0.815</u>	0.205	0.763	0.792	0.232
	DSE	0.750	0.800	<u>0.075</u>	0.740	0.750	0.398	0.732	0.785	<u>0.146</u>	<u>0.799</u>	<u>0.815</u>	0.234	0.753	0.787	0.213
	PE	0.747	0.800	<u>0.075</u>	0.705	0.738	0.164	0.726	0.787	0.161	0.769	0.806	0.037	0.737	0.783	0.109
	KLE-Heat	0.748	0.803	0.112	0.722	0.749	0.243	0.736	0.787	0.176	0.720	0.789	0.233	0.731	0.782	0.191
	KLE-Matern	<u>0.788</u>	<u>0.818</u>	0.082	<u>0.740</u>	0.756	<u>0.038</u>	0.739	0.788	0.144	0.782	0.813	0.037	0.762	<u>0.794</u>	<u>0.075</u>
	UMPIRE	0.773	0.768	0.112	0.753	<u>0.763</u>	0.485	0.752	<u>0.790</u>	0.187	0.796	0.787	0.161	<u>0.768</u>	0.777	0.236
	Cos Eigenscore	0.756	0.713	0.103	0.733	0.709	0.105	0.767	0.784	0.192	0.744	0.747	<u>0.090</u>	0.750	0.738	0.123
	Cov Eigenscore	0.640	0.644	0.406	0.707	0.696	0.133	0.715	0.768	0.166	0.677	0.713	0.416	0.685	0.705	0.280
SGPU (ours)		0.840	0.840	0.020	0.730	0.770	0.020	0.753	0.798	0.150	0.829	0.832	0.099	0.788	0.810	0.072
VQAD	SE	0.681	0.636	0.220	0.703	0.663	0.346	0.734	0.648	0.318	0.647	0.537	0.246	0.691	0.621	0.282
	DSE	0.688	0.638	0.238	0.703	0.658	0.359	0.732	0.643	0.312	0.641	0.457	0.259	0.691	0.599	0.292
	PE	<u>0.723</u>	0.662	0.054	0.692	0.649	<u>0.109</u>	0.731	0.650	0.132	0.672	0.534	0.096	0.705	0.620	<u>0.132</u>
	KLE-Heat	0.677	0.652	0.141	0.677	0.652	0.141	0.727	0.643	0.325	0.496	0.612	0.314	0.644	<u>0.640</u>	0.230
	KLE-Matern	0.720	<u>0.665</u>	0.120	<u>0.720</u>	<u>0.665</u>	0.120	0.729	0.643	0.296	0.567	0.564	<u>0.100</u>	0.684	0.634	0.159
	UMPIRE	0.688	0.597	0.184	0.704	0.617	0.321	0.768	0.654	0.381	<u>0.734</u>	0.621	0.152	<u>0.724</u>	0.622	0.260
	Cos Eigenscore	0.631	0.502	0.176	0.710	0.619	0.194	0.792	0.665	0.193	0.674	0.687	0.240	0.702	0.618	0.201
	Cov Eigenscore	0.654	0.513	0.202	0.684	0.604	0.329	<u>0.771</u>	0.650	0.108	0.672	0.696	0.296	0.695	0.616	0.234
SGPU (ours)		0.770	0.770	<u>0.060</u>	0.730	0.710	0.060	0.750	<u>0.664</u>	0.278	0.758	0.815	0.442	0.752	0.740	0.210
ADVQA	SE	0.688	0.742	0.098	0.657	0.669	0.147	0.630	0.574	0.303	0.716	0.647	0.050	0.673	0.658	0.149
	DSE	0.687	0.741	0.106	0.664	0.673	0.168	0.632	0.572	0.286	0.720	0.649	<u>0.046</u>	0.676	0.659	0.152
	PE	0.693	<u>0.745</u>	0.030	0.655	0.666	0.118	0.630	0.575	0.324	0.711	0.643	0.200	0.672	0.657	0.168
	KLE-Heat	0.724	0.760	0.078	0.715	0.702	0.171	0.615	0.565	0.285	0.700	0.640	0.137	0.688	0.667	0.168
	KLE-Matern	<u>0.724</u>	0.760	0.097	0.718	0.701	<u>0.044</u>	0.628	0.571	<u>0.254</u>	0.730	0.656	0.026	0.700	<u>0.672</u>	0.105
	UMPIRE	0.627	0.659	0.187	0.641	0.631	0.163	<u>0.665</u>	0.583	0.378	<u>0.735</u>	0.613	<u>0.188</u>	0.667	0.621	0.229
	Cos Eigenscore	0.573	0.577	0.080	0.556	0.521	0.130	0.683	0.576	0.380	0.726	<u>0.675</u>	0.212	0.635	0.587	0.201
	Cov Eigenscore	0.575	0.583	0.355	0.613	0.561	0.218	0.637	0.550	0.200	0.656	0.629	0.524	0.620	0.581	0.324
SGPU (ours)		0.740	0.750	0.030	0.690	0.690	0.030	0.655	<u>0.623</u>	0.402	0.757	0.740	0.228	0.711	0.701	0.173
VIZWIZ	SE	0.818	0.607	0.186	0.790	0.649	0.234	0.741	0.702	0.204	0.790	0.671	0.254	0.785	0.670	0.219
	DSE	0.824	0.598	0.214	<u>0.792</u>	0.640	0.249	0.742	0.700	0.183	<u>0.791</u>	0.666	0.276	0.787	0.651	0.230
	PE	0.783	0.586	0.126	0.778	0.639	<u>0.056</u>	0.741	0.706	0.218	0.755	0.650	0.046	0.764	0.645	0.112
	KLE-Heat	0.746	0.566	0.261	0.767	0.635	0.236	0.743	0.701	0.225	0.726	0.632	0.218	0.746	0.634	0.235
	KLE-Matern	0.785	0.592	0.260	0.763	<u>0.652</u>	0.055	0.748	0.703	<u>0.187</u>	0.764	0.657	0.046	0.765	0.651	<u>0.137</u>
	UMPIRE	<u>0.848</u>	0.522	0.120	0.776	0.607	0.214	0.780	<u>0.710</u>	0.244	0.789	0.627	0.182	<u>0.798</u>	0.616	0.193
	Cos Eigenscore	0.790	0.501	<u>0.116</u>	0.763	0.571	0.068	0.794	0.701	0.340	0.760	0.580	0.100	0.777	0.588	0.156
	Cov Eigenscore	0.686	0.572	0.048	0.701	0.533	0.098	0.757	0.685	0.396	0.701	0.546	0.092	0.711	0.588	0.156
SGPU (ours)		0.881	0.872	0.473	0.819	0.808	0.330	<u>0.783</u>	0.777	0.301	0.828	0.814	0.319	0.828	0.819	0.368
Imagenette	SE	0.681	0.593	0.239	0.583	0.573	0.250	0.510	0.733	0.414	0.643	0.570	0.333	0.604	0.617	0.309
	DSE	0.684	0.594	0.188	0.574	0.570	0.224	0.521	0.721	0.433	0.644	0.573	0.296	0.605	0.614	0.285
	PE	0.677	0.598	0.129	0.663	<u>0.647</u>	0.125	0.546	0.750	0.442	0.610	0.569	0.343	0.624	<u>0.641</u>	0.260
	KLE-Heat	0.667	0.584	0.324	0.600	0.581	0.359	0.486	0.714	0.364	0.602	0.585	0.439	0.589	0.616	0.372
	KLE-Matern	0.677	0.589	0.216	0.595	0.578	0.270	0.484	0.714	0.403	0.605	0.582	0.313	0.590	0.616	0.301
	UMPIRE	0.672	0.534	0.250	0.588	0.532	0.299	0.465	0.755	0.375	0.711	0.578	0.427	0.609	0.600	0.338
	Cos Eigenscore	0.700	0.504	0.274	0.679	0.550	0.352	0.507	0.764	0.371	0.612	0.598	0.345	0.625	0.604	0.336
	Cov Eigenscore	0.704	0.501	<u>0.104</u>	0.778	0.614	0.073	0.872	0.551	0.075	0.721	0.638	0.123	0.769	0.576	0.094
SGPU (ours)		0.800	0.790	0.020	0.740	0.740	0.030	0.669	<u>0.761</u>	0.305	0.785	0.805	0.439	0.749	0.774	0.199

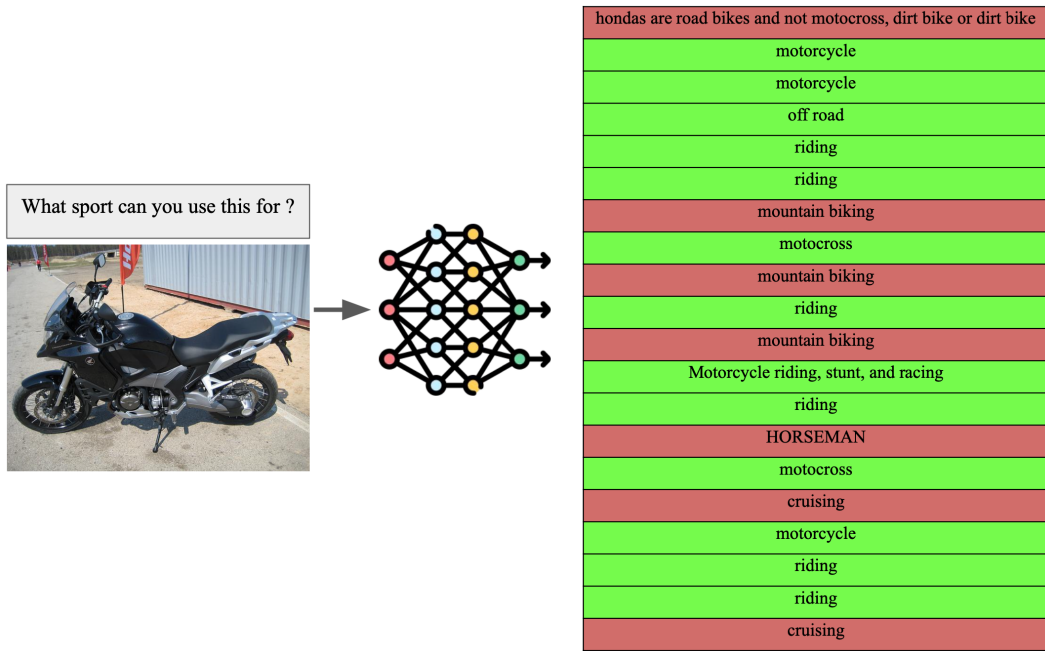


Figure A.5. **LVLM input and answers labeling.** Each answer is labeled with LLM-as-judge method, green means right, red means wrong.

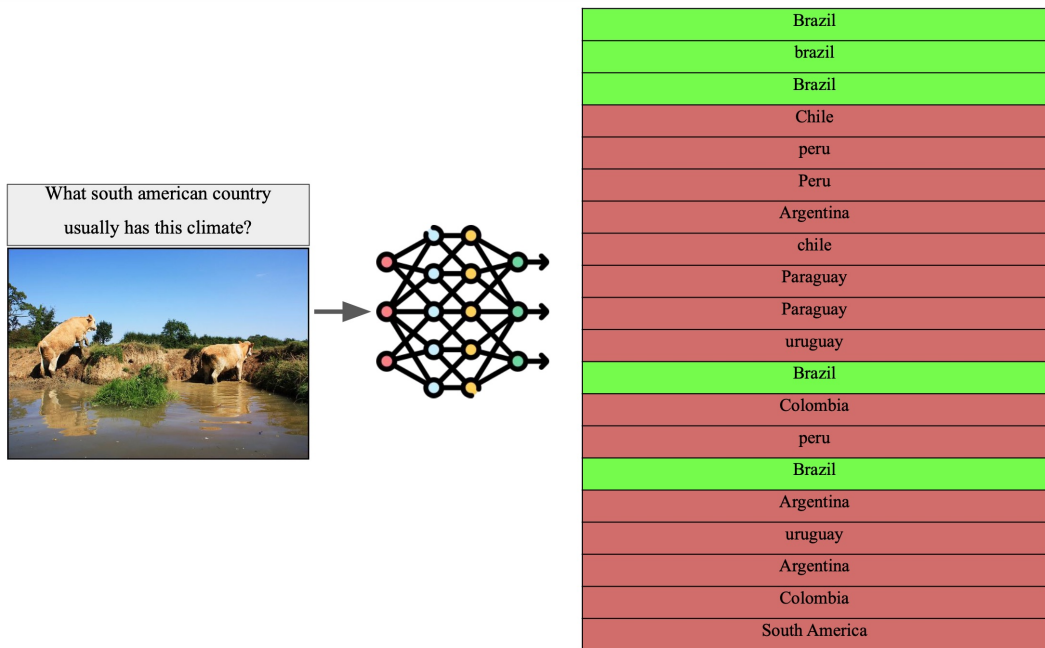


Figure A.6. **LVLM input and answers labeling.** Each answer is labeled with LLM-as-judge method, green means right, red means wrong.